CALCULATING THE RADAR CROSS SECTION OF THE RESISTIVE TARGETS USING THE HAAR WAVELETS

S. Hatamzadeh-Varmazyar

Department of Electrical Engineering
Islamic Azad University
Science and Research Branch, Tehran, Iran

M. Naser-Moghadasi

Central Commission for Scientific
Literacy & Art Societies
Islamic Azad University
Science and Research Branch, Tehran, Iran

E. Babolian

Department of Mathematics
Tarbiat Moallem University
599 Taleghani Avenue, Tehran 15618, Iran

Z. Masouri

Department of Mathematics
Islamic Azad University
Science and Research Branch, Tehran, Iran

Abstract—In this paper, the Haar wavelets basis functions are applied to the method of moments to calculate the radar cross section of the resistive targets. This problem is modeled by the integral equations of the second kind. An effective numerical method for solving these integral equations is proposed. The problem is treated in detail, and illustrative computations are given for several cases. This method can be generalized to apply to objects of arbitrary geometry.

1. INTRODUCTION

The development of numerical methods for solving integral equations in Electromagnetics has attracted intensive researches for more than four decades [1, 2]. The use of high-speed computers allows one to make more computations than ever before. During these years, careful analysis has paved the way for the development of efficient and effective numerical methods and, of equal importance, has provided a solid foundation for a through understanding of the techniques.

Over several decades, electromagnetic scattering problems have been the subject of extensive researches (see [3–54]). Scattering from arbitrary surfaces such as square, cylindrical, circular, spherical [3–9] are commonly used as test cases in computational Electromagnetics, because analytical solutions for scattered fields can be derived for these geometries [3].

An important parameter in scattering studies is the electromagnetic scattering by a target which is usually represented by its *echo area* or *radar cross section* (RCS) [55]. The echo area or RCS is defined as the area intercepting the amount of power that, when scattered isotropically, produces at the receiver a density that is equal to the density scattered by the actual target [56]. For a two-dimensional target the scattering parameter is referred to as the *scattering width* (SW) or alternatively as the *radar cross section per unit length*.

When the transmitter and receiver are at the same location, the RCS is usually referred to as *monostatic* (or *backscattered*) and it is referred to as *bistatic* when the two are at different locations [55]. Observations made toward directions that satisfy Snell's law of reflection are usually referred to as specular. Therefore the RCS of target is very important parameter which characterizes its scattering properties. A plot of the RCS as a function of the space coordinates is usually referred to as the RCS pattern.

Calculating the radar cross section of the resistive targets leads to solve the integral equations of the second kind with complex kernels. Of course, if the resistance of the target approaches to zero, then the problem is modeled by integral equations of the first kind. However, for solving integral equations of the second kind, several numerical approaches have been proposed. These numerical methods often use the basis functions and transform the integral equation to a linear system that can be solved by direct or iterative methods [57]. It is important in these methods to select an appropriate set of basis functions so that the approximate solution of integral equation has a good accuracy.

It is the purpose of this paper to use the Haar wavelets as a set

of orthogonal basis functions and to apply them to the method of moments for calculating the radar cross section of the resistive targets. Using this method, the second kind integral equation reduces to a linear system of algebraic equations. Solving this system gives an approximate solution for these problems.

First of all, an extensive review of wavelets containing the definition, expansion and properties is performed. After this, the electric field integral equation is introduced. Then, the method of moments is proposed for solving integral equations of the second kind using Haar wavelets basis functions. Finally, the problem of calculating the radar cross section of the resistive strips is described in detail and solved by the presented method, and illustrative computations are given for several cases.

2. WAVELET: DEFINITION, EXPANSION, AND PROPERTIES

A wavelet is a "small wave", which has its energy concentrated in time to give a tool for the analysis of transient, nonstationary, or time-varying phenomena [58]. It still has the oscillating wave-like characteristic but also has the ability to allow simultaneous time and frequency analysis with a flexible mathematical function.

In this section, the definition of wavelets and expansion of any function $f(t)$ in terms of these basis functions is presented. Also, some properties of wavelets are surveyed.

2.1. Definition and Expansion

We start by defining the scaling function and then define the wavelet in terms of it.

Let $\mathcal{L}^2(\mathbb{R})$ be the space of square integrable functions. A set of scaling functions in terms of integer translates of the basic *scaling function* or *father wavelet* $\varphi(t)$ is defined by [58]

$$\varphi_k(t) = \varphi(t - k), \qquad k \in \mathbb{Z}, \ \varphi \in \mathcal{L}^2(\mathbb{R}). \tag{1}$$

The subspace of $\mathcal{L}^2(\mathbb{R})$ spanned by these functions is defined as

$$\mathcal{V}_0 = \overline{\underset{k \in \mathbb{Z}}{\mathrm{Span}\{\varphi_k(t)\}}}. \tag{2}$$

This means that

$$f(t) = \sum_k c_k \varphi_k(t) \qquad \text{for any } f(t) \in \mathcal{V}_0. \tag{3}$$

One can generally increase the size of the subspace spanned by changing the time scale of the scaling function. A two-dimensional family of functions is generated from the basic scaling function or father wavelet by scaling and translation by [58]

$$\varphi_{j,\,k}(t) = 2^{j/2}\varphi\left(2^{j}t - k\right), \tag{4}$$

whose span over k is

$$\mathcal{V}_j = \overline{\underset{k\in\mathbb{Z}}{\text{Span}}\{\varphi_k\left(2^j t\right)\}} = \overline{\underset{k\in\mathbb{Z}}{\text{Span}}\{\varphi_{j,\,k}(t)\}}. \tag{5}$$

So, $\{\varphi_{j,\,k}(t)\}_k$ is a basis for $\mathcal{V}_j$. This means that if $f(t) \in \mathcal{V}_j$, then it can be expressed as

$$f(t) = \sum_{k\in\mathbb{Z}} c_k \varphi_{j,\,k}(t), \tag{6}$$

where Eq. (6) represents the projection of the function f onto the subspace of scaling functions or father wavelets at resolution j.

According to the above definitions, it is clear that

$$\mathcal{V}_j \subset \mathcal{V}_{j+1} \qquad \text{for all } j \in \mathbb{Z}. \tag{7}$$

The nesting of the spans of $\varphi(2^j t - k)$, denoted by $\mathcal{V}_j$ and shown in Eq. (7), is achieved by requiring that $\varphi(t) \in \mathcal{V}_1$, which means that if $\varphi(t)$ is in $\mathcal{V}_0$, it is also in $\mathcal{V}_1$, the space spanned by $\varphi(2t)$. This means $\varphi(t)$ can be expressed in terms of a weighted sum of shifted $\varphi(2t)$ as

$$\varphi(t) = \sum_{n\in\mathbb{Z}} h(n)\sqrt{2}\varphi(2t - n), \tag{8}$$

where the sequence $\{h(n)\}$ of real or perhaps complex numbers is called the scaling function or father wavelet coefficients (or the scaling filter or the scaling vector) and the $\sqrt{2}$ maintains the norm of the scaling function with the scale of two.

The Eq. (8) is called the refinement equation, the multiresolution analysis (MRA) equation, or the dilation equation [58, 59]. Now, a different set of functions $\psi_{j,\,k}(t)$ can be defined that span the differences between the spaces spanned by the various scales of the scaling function. These functions are the *mother wavelets*. There are several advantages to requiring that the father wavelets and mother wavelets be orthogonal. Orthogonal basis functions allow simple calculation of expansion coefficients satisfying Parseval's theorem that allows a partitioning of the signal energy in the wavelet transform domain. The

orthogonal complement of $\mathcal{V}_j$ in $\mathcal{V}_{j+1}$ is defined as $\mathcal{W}_j$. This means that all members of $\mathcal{V}_j$ are orthogonal to all members of $\mathcal{W}_j$. We require

$$< \varphi_{j,k}(t), \psi_{j,l}(t) > = \int \varphi_{j,k}(t)\psi_{j,l}(t)dt = 0, \qquad (9)$$

for all appropriate j, $k,l \in \mathbb{Z}$.

The relationship of the various subspaces can be seen from the following expressions. Using Eq. (7) we may start at any $\mathcal{V}_j$, say at $j = 0$, and write

$$\mathcal{V}_0 \subset \mathcal{V}_1 \subset \mathcal{V}_2 \subset \cdots \subset \mathcal{L}^2(\mathbb{R}). \qquad (10)$$

Now, the wavelet spanned subspace $\mathcal{W}_j$ can be defined such that

$$\mathcal{V}_1 = \mathcal{V}_0 \oplus \mathcal{W}_0,$$

which extends to

$$\mathcal{V}_2 = \mathcal{V}_0 \oplus \mathcal{W}_0 \oplus \mathcal{W}_1.$$

In general this gives

$$\mathcal{L}^2 = \mathcal{V}_0 \oplus \mathcal{W}_0 \oplus \mathcal{W}_1 \oplus \ldots, \qquad (11)$$

when $\mathcal{V}_0$ is the initial space spanned by the scaling function $\varphi(t - k)$. Fig. 1 pictorially shows the nesting of the father wavelet spaces $\mathcal{V}_j$ for different scales j and how the mother wavelet spaces are the disjoint differences (except for the zero element) or, orthogonal complements.
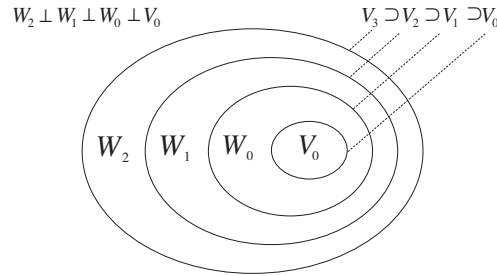

Figure 1. Father wavelet and mother wavelet vector spaces.

The scale of the initial space is arbitrary and could be chosen at a higher resolution of, say, $j = j_0$ to give

$$\mathcal{L}^2 = \mathcal{V}_{j_0} \oplus \mathcal{W}_{j_0} \oplus \mathcal{W}_{j_0+1}, \qquad (12)$$

or at even $j = -\infty$ where Eq. (12) becomes

$$\mathcal{L}^2 = \cdots \oplus \mathcal{W}_{-2} \oplus \mathcal{W}_{-1} \oplus \mathcal{W}_0 \oplus \mathcal{W}_1 \oplus \mathcal{W}_2 \ldots \qquad (13)$$

Since these mother wavelets reside in the space spanned by the next narrower father wavelet, $\mathcal{W}_0 \subset \mathcal{V}_1$, they can be represented by a weighted sum of shifted father wavelet $\varphi(2t)$ defined in Eq. (8) by

$$\psi(t) = \sum_{n \in \mathbb{Z}} h_1(n)\sqrt{2}\varphi(2t - n), \qquad (14)$$

for some sequences of coefficients $\{h_1(n)\}$. It can be shown that the mother wavelet coefficients are required by orthogonality to be related to the father wavelet coefficients by [58, 59]

$$h_1(n) = (-1)^n h(1 - n), \qquad (15)$$

the function generated by (14) gives the mother wavelet $\psi(t)$ for a class of expansion functions of the form

$$\psi_{j,k}(t) = 2^{j/2}\psi\left(2^j t - k\right), \qquad j, k \in \mathbb{Z}, \qquad (16)$$

where, 2^j is the scaling of t, $2^{-j}k$ is the translation in t, and $2^{j/2}$ maintains the $\mathcal{L}^2$ norm of the wavelet at different scales.

The set of these functions is a basis for the space of square integrable functions $\mathcal{L}^2(\mathbb{R})$, i.e.,

$$f(t) = \sum_j \sum_k d_{j,k}\psi_{j,k}(t), \qquad f(t) \in \mathcal{L}^2(\mathbb{R}). \qquad (17)$$

2.2. Some Properties of Wavelets

The wavelet expansion set is not unique. There are many different wavelets systems that can be used effectively, but all seem to have some similar characteristics [58–60].

1. All so-called first-generation wavelet systems are generated from a single scaling function (father wavelet) or mother wavelet by *scaling* and *translation*.

2. The lower resolution coefficients can be calculated from the higher resolution coefficients by a tree-structured algorithm called a *filter bank*. This allows a very efficient calculation of the expansion coefficients.

3. Almost all useful wavelet systems satisfy the *multiresolution* conditions. A *multiresolution analysis* (MRA) is a nested sequence.

$$\cdots \subseteq \mathcal{V}_{-1} \subseteq \mathcal{V}_0 \subseteq \mathcal{V}_1 \subseteq \mathcal{V}_2 \subseteq \ldots$$

of subspaces of $\mathcal{L}^2(\mathbb{R})$ with a scaling function φ such that

i) $\bigcup_{j \in \mathbb{Z}} \mathcal{V}_j$ is dense in $\mathcal{L}^2(\mathbb{R})$,

ii) $\bigcap_{j \in \mathbb{Z}} \mathcal{V}_j = \{0\}$,

iii) $f(t) \in \mathcal{V}_j$ if and only if $f(2^{-j}t) \in \mathcal{V}_0$, and

iv) $\{\varphi(t - k)\}_{k \in \mathbb{Z}}$ is an orthogonal basis for $\mathcal{V}_0$.

4. If the father wavelets and mother wavelets form an orthogonal basis, there is a Parseval's theorem that relates the energy of the signal $f(t)$ to the energy in each of the components and their wavelet coefficients. That is one reason why orthogonality is important.

2.3. The Haar Wavelet System

Wavelets are grouped into families, with names such as the Haar wavelets, the Mexican Hat wavelets, the Shannon wavelets and etc. [60].

If we choose the scaling function to have compact support over $0 \le t \le 1$, then a solution to (8) is a father wavelet as follows [58, 60]:

$$\varphi(t) = \begin{cases} 1, & \text{if } 0 \le t < 1 \\ 0, & \text{otherwise} \end{cases} \tag{18}$$

with only two nonzero coefficients $h(0) = h(1) = 1/\sqrt{2}$ and (14) and (15) require the mother wavelet to be

$$\psi(t) = \begin{cases} 1, & \text{for } 0 \le t < \dfrac{1}{2} \\ -1, & \text{for } \dfrac{1}{2} \le t < 1 \\ 0, & \text{otherwise} \end{cases} \tag{19}$$

with only two nonzero coefficients $h_1(0) = 1/\sqrt{2}$ and $h_1(1) = -1/\sqrt{2}$. Note that the father and mother wavelets are related in the following way:

$$\psi(t) = \varphi(2t) - \varphi(2t - 1). \tag{20}$$

$\mathcal{V}_0$ is the space spanned by $\varphi(t-k)$. The next higher resolution space $\mathcal{V}_1$ is spanned by $\varphi(2t-k)$ which allows a somewhat more interesting class of functions or signals which does include $\mathcal{V}_0$. As we consider higher values of scale j, the space $\mathcal{V}_j$ spanned by $\varphi(2^j t - k)$ becomes more suitable to approximate arbitrary functions or signals.

The Haar wavelets are illustrated in Fig. 2 that shows clearly how increasing the scale allows greater and greater detail to be realized.
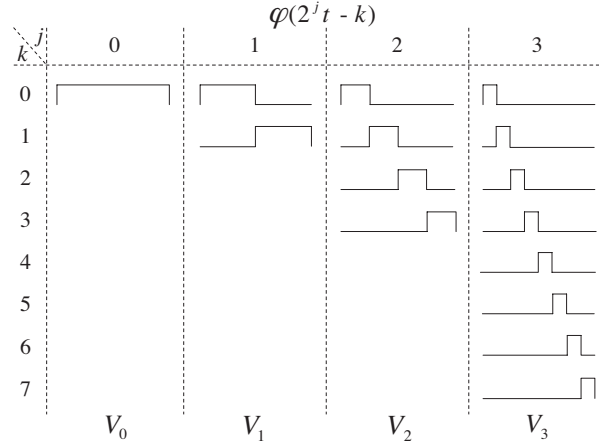
Figure 2. Haar scaling functions that span $\mathcal{V}_j$.

According to the orthogonal decomposition presented in subsection 2.1, for arbitrary scale j we can write

$$\mathcal{V}_{j+1} = \mathcal{V}_j \oplus \mathcal{W}_j, \tag{21}$$

for example, for $\mathcal{V}_3$

$$\mathcal{V}_3 = \mathcal{V}_2 \oplus \mathcal{W}_2. \tag{22}$$

The $\mathcal{V}_2$ can be further decomposed into

$$\mathcal{V}_2 = \mathcal{V}_1 \oplus \mathcal{W}_1. \tag{23}$$

Also, the $\mathcal{V}_1$ can be decomposed as

$$\mathcal{V}_1 = \mathcal{V}_0 \oplus \mathcal{W}_0. \tag{24}$$

By continuing to decompose the space spanned by the scaling function until the space is one constant, the complete decomposition of $\mathcal{V}_3$ is obtained. This is shown in Fig. 3.
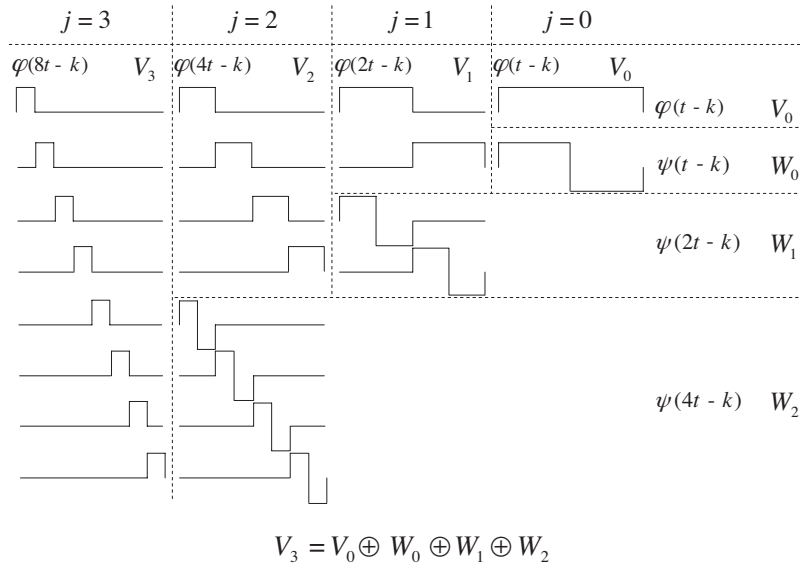
$j = 3$ $j = 2$ $j = 1$ $j = 0$

$\varphi(8t - k)$ V_3 $\varphi(4t - k)$ V_2 $\varphi(2t - k)$ V_1 $\varphi(t - k)$ V_0

$\varphi(t - k)$ V_0

$\psi(t - k)$ W_0

$\psi(2t - k)$ W_1

$\psi(4t - k)$ W_2

$$V_3 = V_0 \oplus W_0 \oplus W_1 \oplus W_2$$

Figure 3. Haar father and mother wavelets decomposition of $\mathcal{V}_3$.

3. ELECTRIC AND MAGNETIC FIELD INTEGRAL EQUATIONS

The key to the solution of any scattering problem is a knowledge of the physical or equivalent current density distributions on the volume or surface of the scatterer. Once these are known then the radiated or scattered fields can be found using the standard radiation integrals. A main objective then of any solution method is to be able to predict accurately the current densities over the scatterer. This can be accomplished by the integral equation (IE) method [55].

In general there are many forms of integral equations. Two of the most popular for time-harmonic Electromagnetics are the *electric field integral equation* (EFIE) and the *magnetic field integral equation* (MFIE). The EFIE enforces the boundary condition on the tangential electric field and the MFIE enforces the boundary condition on the tangential components of the magnetic field. The electric field integral equation will be discussed here.

3.1. Electric Field Integral Equation

The electric field integral equation (EFIE) is based on the boundary condition that the total tangential electric field on a perfectly electric

conducting (PEC) surface of scatterer is zero [55]. This can be expressed as

$$\mathbf{E}_t^t(\mathbf{r} = \mathbf{r}_s) = \mathbf{E}_t^{inc}(\mathbf{r} = \mathbf{r}_s) + \mathbf{E}_t^{scat}(\mathbf{r} = \mathbf{r}_s) = 0 \quad \text{on } S, \qquad (25)$$

or

$$\mathbf{E}_t^{scat}(\mathbf{r} = \mathbf{r}_s) = -\mathbf{E}_t^{inc}(\mathbf{r} = \mathbf{r}_s) \quad \text{on } S, \qquad (26)$$

where, S is the conducting surface of the scatterer and $\mathbf{r} = \mathbf{r}_s$ is the position vector of any point on the surface of the scatterer. The subscript t indicates tangential components.

The incident field that impinges on the surface of the scatterer induces on it an electric current density $\mathbf{J}_s$ which in turn radiates the scattered field. The scattered field everywhere can be found using the following equation [55]:

$$\mathbf{E}^{scat}(\mathbf{r}) = -j\omega\mathbf{A} - j\frac{1}{\omega\mu\epsilon}\nabla(\nabla \cdot \mathbf{A}) = -j\frac{1}{\omega\mu\epsilon}\left[\omega^2\mu\epsilon\mathbf{A} + \nabla(\nabla \cdot \mathbf{A})\right], \qquad (27)$$

where,

ϵ, is the permittivity of the medium;

μ, is the permeability of the medium;

ω, is the angle frequency of the incident field;

∇, is the gradient operator;

$\mathbf{A}$, is the magnetic vector potential, so that

$$\mathbf{A}(\mathbf{r}) = \mu \int\int_S \mathbf{J}_s(\mathbf{r}')\frac{e^{-j\beta R}}{4\pi R}ds', \qquad (28)$$

where, R is the distance from source point to the observation point.

Equations (27) and (28) can also be expressed as [55]

$$\mathbf{E}^{scat}(\mathbf{r}) = -j\frac{\eta}{\beta}\left[\beta^2 \iint_S \mathbf{J}_s(\mathbf{r}')G(\mathbf{r},\mathbf{r}')ds' + \nabla \iint_S \nabla' \cdot \mathbf{J}_s(\mathbf{r}')G(\mathbf{r},\mathbf{r}')ds'\right], \qquad (29)$$

where, η is the intrinsic impedance of the medium and β is the phase constant; $\mathbf{r}$ and $\mathbf{r}'$ are the position vectors of the observation point and source point respectively. also,

$$G(\mathbf{r},\mathbf{r}') = \frac{e^{-j\beta R}}{4\pi R}, \qquad (30)$$

$$R = |\mathbf{r} - \mathbf{r}'|. \qquad (31)$$

In Eq. (29), ∇ and ∇' are, respectively, the gradients with respect to the observation and source coordinates and $G(\mathbf{r}, \mathbf{r}')$ is referred to as Green's function for a three-dimensional scatterer.

If the observations are restricted on the surface of the scatterer ($\mathbf{r} = \mathbf{r}_s$), then Eq. (29) through Eq. (31) can be expressed using Eq. (26) as

$$j\frac{\eta}{\beta}\left[\beta^2 \iint_S \mathbf{J}_s\left(\mathbf{r}'\right) G\left(\mathbf{r}_s, \mathbf{r}'\right) ds' + \nabla \iint_S \nabla' \cdot \mathbf{J}_s\left(\mathbf{r}'\right) G\left(\mathbf{r}_s, \mathbf{r}'\right) ds'\right]$$
$$= \mathbf{E}_t^{inc}\left(\mathbf{r} = \mathbf{r}_s\right). \tag{32}$$

Because the right side of Eq. (32) is expressed in terms of the known incident electric field, it is referred to as the *electric field integral equation* (EFIE). It can be used to find the current density $\mathbf{J}_s(\mathbf{r}')$ at any point $\mathbf{r} = \mathbf{r}'$ on the scatterer. It should be noted that Eq. (32) is actually an integro-differential equation, but usually it is referred to as an integral equation.

Equation (32) is a general surface EFIE for three-dimensional problems and its form can be simplified for two-dimensional geometries. Note that this equation gives the EFIE for conducting surfaces. EFIE for the resistive surfaces will be described in detail in Section 5.

4. IMPLEMENTING THE METHOD OF MOMENTS USING HAAR WAVELETS

In this section, we apply Haar wavelets as orthogonal basis functions to solve the integral equations of the second kind by moments method.

Consider the following Fredholm integral equation of the second kind:

$$x(s) + \int_a^b k(s,t)x(t)dt = y(s), \tag{33}$$

where, $k(s,t)$ and $y(s)$ are known functions but $x(t)$ is unknown. We can select a sequence of finite dimensional subspaces $\mathcal{V}_j \subset \mathcal{L}^2(\mathbb{R})$, $j \geq 1$. Let $\{\varphi_{n,k}\}_{k=1}^n$ be a wavelet basis for $\mathcal{V}_j$ in which, $n = 2^j$. Moreover, $k(s,t) \in \mathcal{L}^2([a, b) \times [a, b))$ and $y(s) \in \mathcal{L}^2([a, b))$. Approximating the function $x(s)$ with respect to the basis functions by (6) gives

$$x(s) \simeq \sum_{k=1}^n c_k \varphi_{n,k}(s), \tag{34}$$

such that the c_ks are wavelet coefficients of $x(s)$ that should be determined.

Substituting Eq. (34) into (33) follows:

$$\sum_{k=1}^{n} c_k \varphi_{n,\,k}(s) + \sum_{k=1}^{n} c_k \int_a^b k(s,\,t)\varphi_{n,\,k}(t)dt \simeq y(s). \qquad (35)$$

Now, let s_i, $i = 1, 2, \ldots, n$, be n appropriate points in interval $[a, b]$; putting $s = s_i$ in Eq. (35) follows:

$$\sum_{k=1}^{n} c_k \varphi_{n,\,k}(s_i) + \sum_{k=1}^{n} c_k \int_a^b k(s_i,\,t)\varphi_{n,\,k}(t)dt \simeq y(s_i),$$
$$i = 1, 2, \ldots, n, \qquad (36)$$

or

$$\sum_{k=1}^{n} c_k \left[\varphi_{n,\,k}(s_i) + \int_a^b k(s_i,\,t)\varphi_{n,\,k}(t)dt \right] \simeq y(s_i),$$
$$i = 1, 2, \ldots, n. \qquad (37)$$

Now, replace $\simeq$ with $=$, hence Eq. (37) is a linear system of n algebraic equations for n unknown coefficients $c_1, c_2, \ldots, c_n$. So, an approximate solution $x(s) \simeq \sum_{k=1}^{n} c_k \varphi_{n,\,k}(s)$, is obtained for Eq. (33).

5. CALCULATING THE RADAR CROSS SECTION OF THE RESISTIVE STRIPS

Now, the problem of calculating the RCS of the resistive strips is solved using the presented approach. In Fig. 4, there is a resistive strip that is very long in the $\pm z$ direction. This strip is encountered by an incoming plane wave that has a polarization with its electric field parallel to the z-axis. The magnetic field of this wave is entirely in the x-y plane, and is therefore transverse to the z-axis. It is called transverse magnetic (TM) polarized wave. This polarization therefore produces a current on the strip that flows along the z-axis.

The magnetic vector potential of the current flowing along the strip is given by [61]

$$A_z = \frac{\mu_0}{4j} \int_{-a/2}^{a/2} I_z\left(x'\right) H_0^{(2)}\left(k|x - x'|\right) dx', \qquad (38)$$

where,

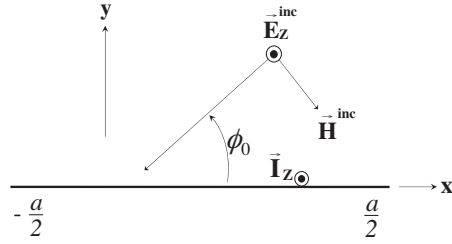$k = \frac{2\pi}{\lambda}$, is free space wave number;

Figure 4. A resistive strip of width a is encountered by an incoming TM-polarized plane wave.

λ, is the wave length;

$\mu_0 = 4\pi \times 10^{-7}$ H/m, is free space permeability;

$G(x, x') = \frac{1}{4j} H_0^{(2)}(k|x - x'|)$, is 2D free space Green's function;

$H_0^{(2)}(x)$, is a Hankel function of the second kind of zero order.

So, the electric field is given by

$$E_z(x) = j\omega A_z(x), \tag{39}$$

or

$$E(x) = \frac{\omega \mu_0}{4} \int_{-a/2}^{a/2} I_z\left(x'\right) H_0^{(2)}\left(k|x - x'|\right) dx'. \tag{40}$$

Assume that $R_s(x)$ is the surface resistance of the strip and note that the units of surface resistance are in Ω/m^2. The boundary condition at the surface of a thin resistive strip is given by the following equation [61]:

$$-E^{inc} = E^{scat} + R_s(x)J(x), \tag{41}$$

where,

$J(x)$, is the surface current of the strip;

E^{scat}, is the scattered electric field produced by the surface current.

Assuming $E^{inc} = e^{jkx \cos\phi_0}$, from Eq. (40) and Eq. (41) it follows:

$$R_s(x)I(x) + \frac{\omega \mu_0}{4} \int_{-a/2}^{a/2} I\left(x'\right) H_0^{(2)}\left(k|x - x'|\right) dx' = -e^{jkx \cos\phi_0}, \tag{42}$$

where, $I(x)$ is the current of the strip.

Equation (42) can be converted to the following equation:

$$h(x) + \int_a^b G\left(x, x'\right) h\left(x'\right) dx' = g(x), \qquad (43)$$

where,

$h(x) = I(x);$

$G(x, x') = \frac{\omega \mu_0}{4} \frac{1}{R_s(x)} H_0^{(2)}\left(k|x - x'|\right);$

$g(x) = -\frac{1}{R_s(x)} e^{jkx \cos \phi_0}.$

It is a Fredholm integral equation of the second kind and can be solved by the presented method. However, from Eq. (42) $I(x)$ can be obtained and then the RCS of the strip can be computed easily.

RCS in two dimensions is defined mathematically as [61]

$$\sigma(\phi) = \lim_{r \to \infty} 2\pi r \frac{|\mathbf{E}^{scat}|^2}{|\mathbf{E}^{inc}|^2}. \qquad (44)$$

In two dimensions, the free space Green's function is

$$G\left(\mathbf{r}, \mathbf{r}'\right) = \frac{1}{4j} H_0^{(2)}\left(k|\mathbf{r} - \mathbf{r}'|\right). \qquad (45)$$

The magnetic vector potential in two-dimensional space is

$$\mathbf{A}(\mathbf{r}) = \mu \iint \mathbf{J}\left(\mathbf{r}'\right) G\left(\mathbf{r}, \mathbf{r}'\right) ds'. \qquad (46)$$

The electric field is given by

$$\mathbf{E} = j\omega \mathbf{A}. \qquad (47)$$

Combining (45), (46), and (47) we obtain

$$\mathbf{E}(\mathbf{r}) = \frac{\omega \mu}{4} \iint \mathbf{J}\left(\mathbf{r}'\right) H_0^{(2)}\left(k|\mathbf{r} - \mathbf{r}'|\right) ds'. \qquad (48)$$

In the TM situation, the incident electric field along the strip is $1\,\mathrm{V/m}$ ($|\mathbf{E}^{inc}|^2 = 1$). So, the denominator of Eq. (44) is unity. This allows us to turn our attention to the numerator. To evaluate (48), we note that as $r \longrightarrow \infty$, we can use the large argument approximation for the Hankel function [61]

$$H_0^{(2)}(r) \approx \sqrt{\frac{2}{\pi r}} e^{-j\left(r - \frac{\pi}{4}\right)}. \qquad (49)$$

Substituting this into (48) and implementing Eq. (44) for the TM case, we obtain

$$\sigma(\phi) = \frac{k\eta^2}{4} \left| \int_{strip} I\left(x', y'\right) e^{jk(x'\cos\phi + y'\sin\phi)} dl' \right|^2. \tag{50}$$

where, $\eta = 376.73\,\Omega$.

In the presented case, the strip is restricted to the x-axis, which simplifies Eq. (50)

$$\sigma(\phi) = \frac{k\eta^2}{4} \left| \int_{-a/2}^{a/2} I\left(x'\right) e^{jkx'\cos\phi} dx' \right|^2. \tag{51}$$

Also, it is possible to define a logarithmic quantity with respect to the RCS, so that

$$\sigma_{dBlm} = 10\log_{10}\sigma. \tag{52}$$

5.1. Uniform Resistance Distribution

Assume that the $R_s(x)$ has a uniform value in throughout of the surface of strip. Considering Eq. (42), $I(x)$ is computed for R_s of 0, 500, 1000 (Ω/m^2), $\phi_0 = \frac{\pi}{2}$, $a = 6\lambda\,(m)$ and $f = 0.3\,GHz$, and then RCS is obtained of Eqs. (51) and (52). The current distributions of the resistive strip for these values of R_s are shown in Figs. 5–8.
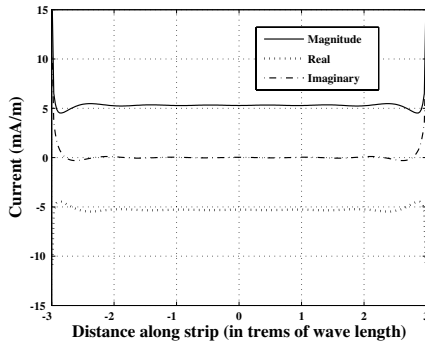
Figure 5. Current distribution across a $6 - \lambda$ strip created by a TM-polarized plane wave for $R_s = 0$ and $f = 0.3\,GHz$.
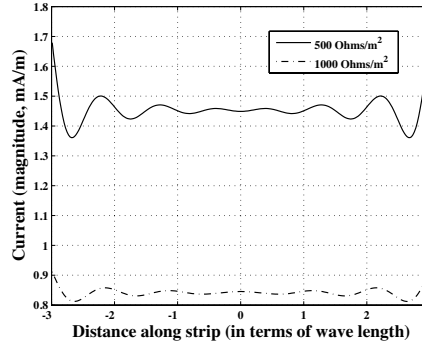
Figure 6. Current magnitude across the $6 - \lambda$ resistive strip for R_s of 500 and 1000 (Ω/m^2) and $f = 0.3\,GHz$.
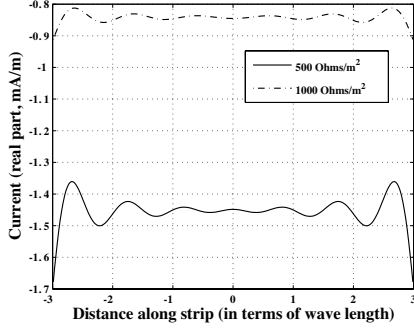
Figure 7. The real part of current across the $6 - \lambda$ resistive strip for R_s of 500 and 1000 (Ω/m^2) and $f = 0.3\,\text{GHz}$.
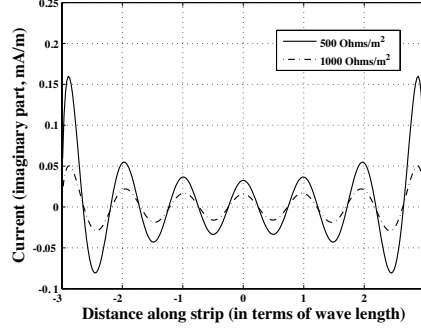

Figure 8. The imaginary part of current across the $6 - \lambda$ resistive strip for R_s of 500 and 1000 (Ω/m^2) and $f = 0.3\,\text{GHz}$.

In Figs. 9 and 10, the bistatic RCS of the $6 - \lambda$ resistive strip, for R_s of 0, 500, 1000 (Ω/m^2) and for $\phi_0 = \frac{\pi}{2}$, $\frac{2\pi}{3}$ has been shown. Also, in Fig. 11 the monostatic RCS of this strip is given. It is seen that the level of the first side lobe is nearly 13 dB down from the main lobe.
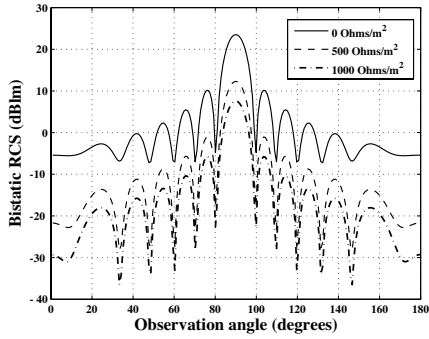
Figure 9. The bistatic RCS of the $6 - \lambda$ resistive strip for R_s of 0, 500, 1000 (Ω/m^2) and $\phi_0 = \frac{\pi}{2}$.
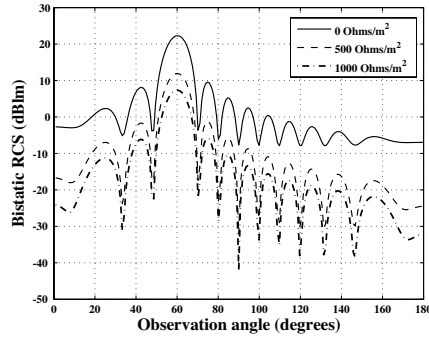
Figure 10. The bistatic RCS of the $6 - \lambda$ resistive strip for R_s of 0, 500, 1000 (Ω/m^2) and $\phi_0 = \frac{2\pi}{3}$.
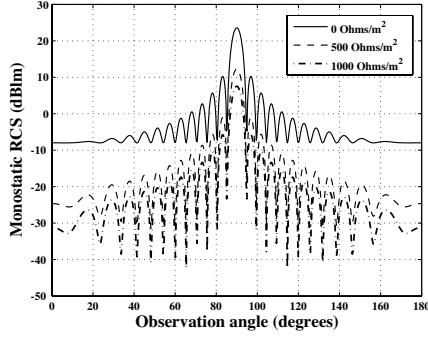
Figure 11. The monostatic RCS of the $6 - \lambda$ resistive strip for R_s of 0, 500, 1000 (Ω/m^2).
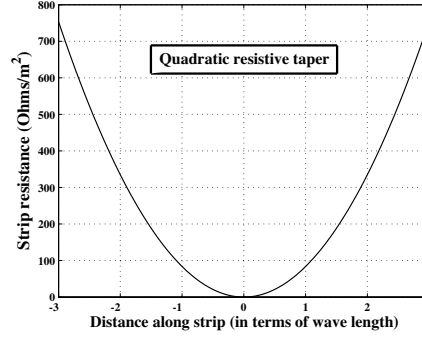

Figure 12. The quadratic taper of a $6 - \lambda$ resistive strip for $k = 2$.
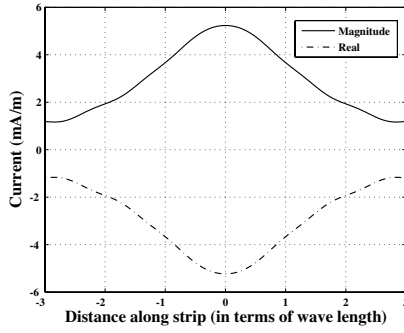

Figure 13. The magnitude and real part of current across the $6 - \lambda$ resistive strip of Fig. 12 for $k = 2$ and $f = 0.3\,\mathrm{GHz}$.
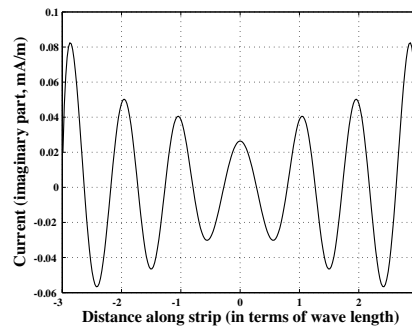

Figure 14. The imaginary part of current across the $6 - \lambda$ resistive strip of Fig. 12 for $k = 2$ and $f = 0.3\,\mathrm{GHz}$.

5.2. Quadratic Resistive Taper

Consider a quadratic resistive taper expressed by

$$R_s(x) = 2\eta \left(\frac{kx}{a} \right)^2 \qquad (\Omega/\mathrm{m}^2), \qquad (53)$$

where, k is a real coefficient.

Figure 12 shows the quadratic taper of a $6 - \lambda$ strip for $k = 2$. After computing $I(x)$ by Eq. (42), the RCS of this strip can be obtained. For $\phi_o = \frac{\pi}{2}$, the magnitude, real part and imaginary part of strip current are shown in Figs. 13 and 14, and the bistatic radar cross section of this

strip shown in Figs. 15 and 16 has been calculated for $k = 0.5$, 1, 2, $\phi_0 = \frac{\pi}{2}$, $\frac{\pi}{4}$, and $f = 0.3\,\text{GHz}$. Fig. 17 shows the monostatic RCS. It is seen that the quadratic taper reduces the first side lobe to a level of $-23\,\text{dB}$ below the main lobe. This taper has reduced the first side lobe by $10\,\text{dB}$, compared with a uniform distribution.
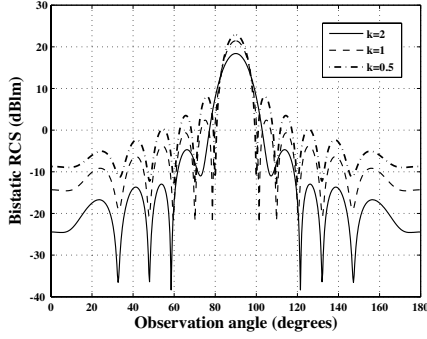
Figure 15. The bistatic RCS of the $6 - \lambda$ resistive strip of Fig. 12 for $k = 0.5$, 1, 2 and $\phi_0 = \frac{\pi}{2}$.
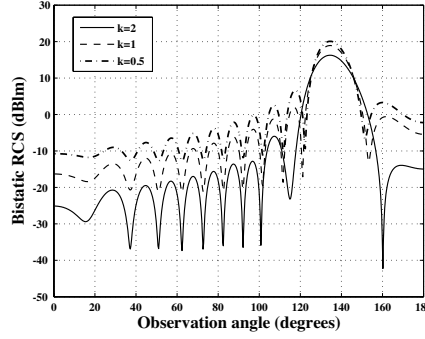
Figure 16. The bistatic RCS of the $6 - \lambda$ resistive strip of Fig. 12 for $k = 0.5$, 1, 2 and $\phi_0 = \frac{\pi}{4}$.
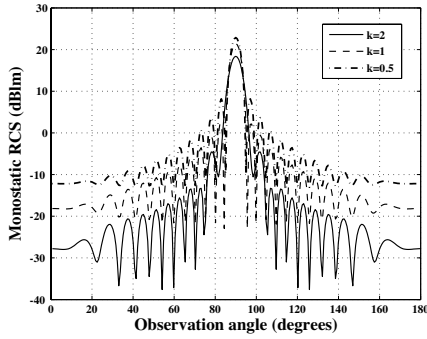
Figure 17. The monostatic RCS of the $6-\lambda$ resistive strip of Fig. 12 for $k = 0.5$, 1, 2.
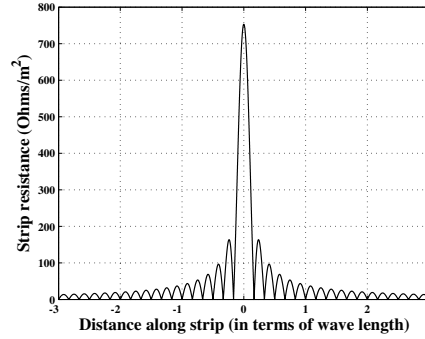
Figure 18. Sinc form resistance distribution of a $6 - \lambda$ resistive strip for $k = 1$.

5.3. Sinc Form Resistance Distribution

In this subsection the problem of determining the scattered fields is solved for a resistive strip of a sinc form resistance distribution shown in Fig. 18.

Consider a sinc form resistance expressed by

$$R_s(x) = 2\eta \left| \frac{\sin k\pi ax}{k\pi ax} \right| \qquad (\Omega/\text{m}^2), \qquad (54)$$

in which, k is a real coefficient.

Applying Eq. (42) to this case gives the current distribution which has been shown in Fig. 19. Then, the bistatic RCS of this case is obtained of Eqs. (51) and (52). Figure 20 shows the results for $k = 0.8,\ 3,\ 30$ and $f = 0.3\,\text{GHz}$.

For $k = 30$, the level of the first side lobe is nearly $13\,\text{dB}$ down from the main lobe.
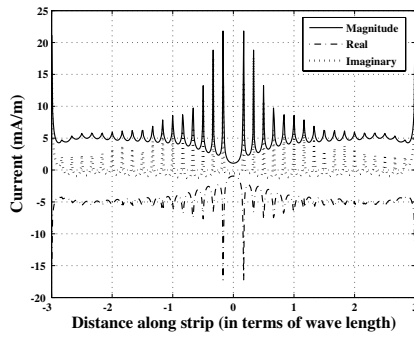

Figure 19. Current across the $6 - \lambda$ resistive strip of Fig. 18 for $k = 1$ and $f = 0.3\,\text{GHz}$.
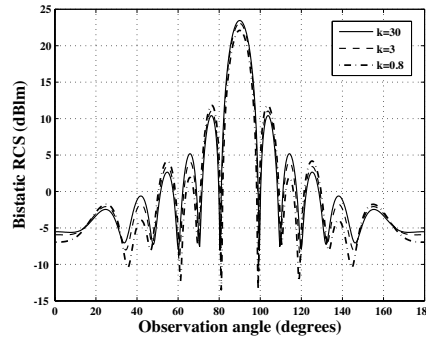
Figure 20. The bistatic RCS of the $6 - \lambda$ resistive strip of Fig. 18 for $k = 0.8,\ 3,\ 30$ and $\phi_0 = \frac{\pi}{2}$.

5.4. Exponential Distribution

The final case is an exponential form distribution of the strip resistance which is defined below:

$$R_s(x) = 2\eta \left(\frac{kx}{a} \right)^2 \exp\left(-\left| \frac{kx}{a} \right| \right) \qquad (\Omega/\text{m}^2). \qquad (55)$$

Figure 21 shows the exponential form resistance distribution of a $6 - \lambda$ strip for $k = 1$. Current distribution of this case for $k = 1$ is shown in Fig. 22, and its bistatic RCS for $k = 0.5,\ 1,\ 1.5$ and $f = 0.3\,\text{GHz}$ is shown in Fig. 23.
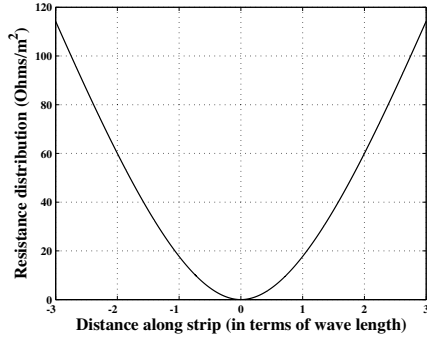
Figure 21. Exponential resistance distribution of a $6 - \lambda$ resistive strip for $k = 1$.
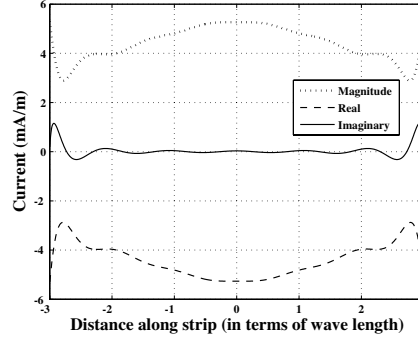
Figure 22. Current across the $6 - \lambda$ resistive strip of Fig. 21 for $k = 1$ and $f = 0.3\,\mathrm{GHz}$.
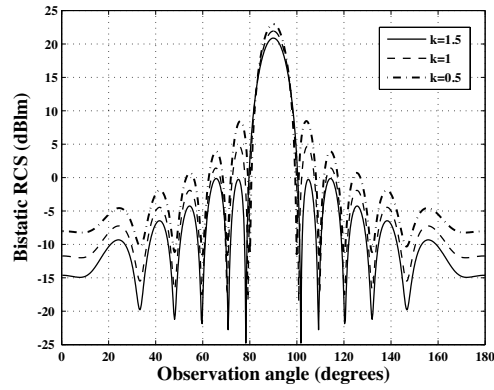

Figure 23. The bistatic RCS of the $6 - \lambda$ resistive strip of Fig. 21 for $k = 0.5,\ 1,\ 1.5$ and $\phi_0 = \frac{\pi}{2}$.

6. CONCLUSION

The presented method in this paper is applied to solve the integral equations of the second kind arising in problem of calculating the radar cross section of the resistive targets based on the method of moments and using the Haar wavelets basis functions.

As the numerical results showed, this method reduces an integral equation of the second kind to a linear system of algebraic equations.

The problem of calculating the RCS of the resistive strips was treated in detail, and illustrative computations were given for several cases.

A comparison of the method presented here with other methods that we have implemented using the block-pulse or triangular basis functions [28,31] shows the accuracy and validity of the presented method.

This method can be easily generalized to apply to objects of arbitrary geometry and arbitrary material.

REFERENCES

1. Wilton, D. R. and C. M. Butler, "Effective methods for solving integral and integro-differential equations," *Electromagnetics*, Vol. 1, 289–308, 1981.

2. Harrington, R. F., "Matrix methods for field problems," *Proc. IEEE*, Vol. 55, No. 2, 136–149, 1967.

3. Mishra, M. and N. Gupta, "Monte Carlo integration technique for the analysis of electromagnetic scattering from conducting surfaces," *Progress In Electromagnetics Research*, PIER 79, 91–106, 2008.

4. Arnold, M. D., "An efficient solution for scattering by a perfectly conducting strip grating," *Journal of Electromagnetic Waves and Applications*, Vol. 20, No. 7, 891–900, 2006.

5. Zhao, J. X., "Numerical and analytical formulations of the extended MIE theory for solving the sphere scattering problem," *Journal of Electromagnetic Waves and Applications*, Vol. 20, No. 7, 967–983, 2006.

6. Ruppin, R., "Scattering of electromagnetic radiation by a perfect electromagnetic conductor sphere," *Journal of Electromagnetic Waves and Applications*, Vol. 20, No. 12, 1569–1576, 2006.

7. Ruppin, R., "Scattering of electromagnetic radiation by a perfect electromagnetic conductor cylinder," *Journal of Electromagnetic Waves and Applications*, Vol. 20, No. 13, 1853–1860, 2006.

8. Hussein, K. F. A., "Efficient near-field computation for radiation and scattering from conducting surfaces of arbitrary shape," *Progress In Electromagnetics Research*, PIER 69, 267–285, 2007.

9. Hussein, K. F. A., "Fast computational algorithm for EFIE applied to arbitrarily-shaped conducting surfaces," *Progress In Electromagnetics Research*, PIER 68, 339–357, 2007.

10. Kishk, A. A., "Electromagnetic scattering from composite objects using a mixture of exact and impedance boundary conditions," *IEEE Transactions on Antennas and Propagation*, Vol. 39, No. 6, 826–833, 1991.

11. Caorsi, S., A. Massa, and M. Pastorino, "A numerical solution to full-vector electromagnetic scattering by three-dimensional nonlinear bounded dielectrics," *IEEE Transactions on Microwave Theory and Techniques*, Vol. 43, No. 2, 428–436, 1995.

12. Shore, R. A. and A. D. Yaghjian, "Dual-surface integral equations in electromagnetic scattering," *IEEE Transactions on Antennas and Propagation*, Vol. 53, No. 5, 1706–1709, 2005.

13. Ylä-Oijala, P. and M. Taskinen, "Well-conditioned Müller formulation for electromagnetic scattering by dielectric objects," *IEEE Transactions on Antennas and Propagation*, Vol. 53, No. 10, 3316–3323, 2005.

14. Li, L. W., P. S. Kooi, Y. L. Qin, T. S. Yeo, and M. S. Leong, "Analysis of electromagnetic scattering of conducting circular disk using a hybrid method," *Progress In Electromagnetics Research*, PIER 20, 101–123, 1998.

15. Liu, Y. and K. J. Webb, "On detection of the interior resonance errors of surface integral boundary conditions for electromagnetic scattering problems," *IEEE Transactions on Antennas and Propagation*, Vol. 49, No. 6, 939–943, 2001.

16. Kishk, A. A., "Electromagnetic scattering from transversely corrugated cylindrical structures using the asymptotic corrugated boundary conditions," *IEEE Transactions on Antennas and Propagation*, Vol. 52, No. 11, 3104–3108, 2004.

17. Tong, M. S. and W. C. Chew, "Nyström method with edge condition for electromagnetic scattering by 2D open structures," *Progress In Electromagnetics Research*, PIER 62, 49–68, 2006.

18. Valagiannopoulos, C. A., "Closed-form solution to the scattering of a skew strip field by metallic pin in a slab," *Progress In Electromagnetics Research*, PIER 79, 1–21, 2008.

19. Frangos, P. V. and D. L. Jaggard, "Analytical and numerical solution to the two-potential Zakharov-Shabat inverse scattering problem," *IEEE Transactions on Antennas and Propagation*, Vol. 40, No. 4, 399–404, 1992.

20. Barkeshli, K. and J. L. Volakis, "Electromagnetic scattering from thin strips — Part II: Numerical solution for strips of arbitrary size," *IEEE Transactions on Education*, Vol. 47, No. 1, 107–113, 2004.

21. Collino, F., F. Millot, and S. Pernet, "Boundary-integral methods for iterative solution of scattering problems with variable impedance surface condition," *Progress In Electromagnetics Research*, PIER 80, 1–28, 2008.

22. Zahedi, M. M. and M. S. Abrishamian, "Scattering from semi-elliptic channel loaded with impedance elliptical cylinder," *Progress In Electromagnetics Research*, PIER 79, 47–58, 2008.

23. Zaki, K. A. and A. R. Neureuther, "Scattering from a perfectly conducting surface with a sinusoidal height profile: TE polarization," *IEEE Transactions on Antennas and Propagation*, Vol. 19, No. 2, 208–214, 1971.

24. Carpentiery, B., "Fast iterative solution methods in electromagnetic scattering," *Progress In Electromagnetics Research*, PIER 79, 151–178, 2008.

25. Du, Y., Y. L. Luo, W. Z. Yan, and J. A. Kong, "An electromagnetic scattering model for soybean canopy," *Progress In Electromagnetics Research*, PIER 79, 209–223, 2008.

26. Umashankar, K. R., S. Nimmagadda, and A. Taflove, "Numerical analysis of electromagnetic scattering by electrically large objects using spatial decomposition technique," *IEEE Transactions on Antennas and Propagation*, Vol. 40, No. 8, 867–877, 1992.

27. Gokten, M., A. Z. Elsherbeni, and E. Arvas, "Electromagnetic scattering analysis using the two-dimensional MRFD formulation," *Progress In Electromagnetics Research*, PIER 79, 387–399, 2008.

28. Hatamzadeh-Varmazyar, S., M. Naser-Moghadasi, E. Babolian, and Z. Masouri, "Numerical approach to survey the problem of electromagnetic scattering from resistive strips based on using a set of orthogonal basis functions," *Progress In Electromagnetics Research*, PIER 81, 393–412, 2008.

29. Hatamzadeh-Varmazyar, S., M. Naser-Moghadasi, and Z. Masouri, "A moment method simulation of electromagnetic scattering from conducting bodies," *Progress In Electromagnetics Research*, PIER 81, 99–119, 2008.

30. Hatamzadeh-Varmazyar, S. and M. Naser-Moghadasi, "New numerical method for determining the scattered electromagnetic fields from thin wires," *Progress In Electromagnetics Research B*, Vol. 3, 207–218, 2008.

31. Hatamzadeh-Varmazyar, S. and M. Naser-Moghadasi, "An integral equation modeling of electromagnetic scattering from the surfaces of arbitrary resistance distribution," *Progress In Electromagnetics Research B*, Vol. 3, 157–172, 2008.

32. Abd-El-Ranouf, H. E. and R. Mittra, "Scattering analysis of dielectric coated cones," *Journal of Electromagnetic Waves and Applications*, Vol. 21, No. 13, 1857–1871, 2007.

33. Choi, S. and N.-H. Myung, "Scattering analysis of open-ended cavity with inner object," *Journal of Electromagnetic Waves and Applications*, Vol. 21, No. 12, 1689–1702, 2007.

34. Li, Y.-L., J.-Y. Huang, and S.-H. Gong, "The scattering cross section for a target irradiated by time-varying electromagnetic waves," *Journal of Electromagnetic Waves and Applications*, Vol. 21, No. 9, 1265–1271, 2007.

35. Rui, P.-L. and R. Chen, "Implicity restarted gmres fast Fourier transform method for electromagnetic scattering," *Journal of Electromagnetic Waves and Applications*, Vol. 21, No. 7, 973–976, 2007.

36. Nashia, N., J. S. Kot, and S. S. Vinogradov, "Scattering by a luneberg lens partially covered by a metallic cap," *Journal of Electromagnetic Waves and Applications*, Vol. 21, No. 4, 549–563, 2007.

37. Yuan, H.-W., S.-X. Gong, X. Wang, and W.-T. Wang, "Scattering analysis of a printed dipole antenna using PBG structures," *Progress In Electromagnetics Research B*, Vol. 1, 189–195, 2008.

38. Faghihi, F. and H. Heydari, "A combination of time domain finite element-boundary integral and with time domain physical optics for calculation of electromagnetic scattering of 3-D structures," *Progress In Electromagnetics Research*, PIER 79, 463–474, 2008.

39. Ahmed, S. and Q. A. Naqavi, "Electromagnetic scattering from a perfect electromagnetic conductor cylinder buried in a dielectric half-space," *Progress In Electromagnetics Research*, PIER 78, 25–38, 2008.

40. Valagiannopoulos, C. A., "Electromagnetic scattering from two eccentric metamaterial cylinders with frequency-dependent permittivities differing slightly each other," *Progress In Electromagnetics Research B*, Vol. 3, 23–34, 2008.

41. Hady, L. K. and A. A. Kishk, "Electromagnetic scattering from conducting circular cylinder coated by meta-materials and loaded with helical strips under oblique incidence," *Progress In Electromagnetics Research B*, Vol. 3, 189–206, 2008.

42. Zainud-Deen, S. H., A. Z. Botros, and M. S. Ibrahim, "Scattering from bodies coated with metamaterial using FDFD method," *Progress In Electromagnetics Research B*, Vol. 2, 279–290, 2008.

43. Li, Y.-L., J.-Y. Huang, M.-J. Wang, and J. Zhang, "Scattering field for the ellipsoidal targets irradiated by an electromagnetic wave with arbitrary polarizing and propagating direction," *Progress In Electromagnetics Research Letters*, Vol. 1, 221–235, 2008.

44. Xu, L., Y.-C. Guo, and X.-W. Shi, "Dielectric half space model for the analysis of scattering from objects on ocean surface," *Journal of Electromagnetic Waves and Applications*, Vol. 21, No. 15, 2287–2296, 2007.

45. Zhong, X. J., T. Cui, Z. Li, Y.-B. Tao, and H. Lin, "Terahertz-wave scattering by perfectly electrical conducting objects," *Journal of Electromagnetic Waves and Applications*, Vol. 21, No. 15, 2331–2340, 2007.

46. Li, Y.-L., J.-Y. Huang, and M.-J. Wang, "Scattering cross section for airborne and its application," *Journal of Electromagnetic Waves and Applications*, Vol. 21, No. 15, 2341–2349, 2007.

47. Wang, M. Y., J. Xu, J. Wu, Y. Yan, and H.-L. Li, "FDTD study on scattering of metallic column covered by double-negative metamaterial," *Journal of Electromagnetic Waves and Applications*, Vol. 21, No. 14, 1905–1914, 2007.

48. Liu, X.-F., B. Z. Wang, and S.-J. Lai, "Element-free Galerkin method in electromagnetic scattering field computation," *Journal of Electromagnetic Waves and Applications*, Vol. 21, No. 14, 1915–1923, 2007.

49. Du, P., B. Z. Wang, H. Li, and G. Zheng, "Scattering analysis of large-scale periodic structures using the sub-entire domain basis function method and characteristic function method," *Journal of Electromagnetic Waves and Applications*, Vol. 21, No. 14, 2085–2094, 2007.

50. Tuz, V. R., "Three-dimensional Gaussian beam scattering from a periodic sequence of bi-isotropic and material layers," *Progress In Electromagnetics Research B*, Vol. 7, 53–73, 2008.

51. Sukharevsky, O. I. and V. A. Vasilets, "Scattering of reflector antenna with conic dielectric radome," *Progress In Electromagnetics Research B*, Vol. 4, 159–169, 2008.

52. Wang, M.-J., Z.-S. Wu, and Y. L. Li, "Investigation on the scattering characteristics of Gaussian beam from two dimensional dielectric rough surfaces based on the Kirchhoff approximation," *Progress In Electromagnetics Research B*, Vol. 4, 223–235, 2008.

53. Sun, X. and H. Ha, "Light scattering by large hexagonal column with multiple densely packed inclusions," *Progress In Electromagnetics Research Letters*, Vol. 3, 105–112, 2008.

54. Kokkorakis, G. C., "Scalar equations for scattering by rotationally symmetric radially inhomogeneous anisotropic sphere," *Progress In Electromagnetics Research Letters*, Vol. 3, 179–186, 2008.

55. Balanis, C. A., *Advanced Engineering Electromagnetics*, Wiley,

New York, 1989.

56. Balanis, C. A., *Antenna Theory: Analysis and Design*, Wiley, New York, 1982.

57. Delves, L. M. and J. L. Mohamed, *Computational Methods for Integral Equations*, Cambridge University Press, Cambridge, 1985.

58. Burrus, C. S., R. A. Gopinath, and H. Guo, *Introduction to Wavelets and Wavelet Transforms*, New Jersey, Prentice Hall, 1998.

59. Daubechies, I., *Ten Lectures on Wavelets*, SIAM, Philadelphia, 1992.

60. Aboufadel, E. and S. Schlicker, *Discovering Wavelets*, John Wiley & Sons, 1999.

61. Bancroft, R., *Understanding Electromagnetic Scattering Using the Moment Method*, Artech House, London, 1996.